Paper presented at the 13th Topical Meeting on the Technology of Fusion Power, June 7-11, 1998,Nashville, Tennessee.
---------- **DRAFT**----------

X-RAYS SURFACE AND VOLUMETRIC HEAT DEPOSITION AND TRITIUM BREEDING ISSUES IN LIQUID-PROTECTED FW IN HIGH POWER DENSITY DEVICES

Mahmoud Z. Youssef, Neil Morley, and Anter El-Azab

School of Engineering and Applied Science,
University of California at Ls Angeles
Los Angeles, CA, 90095, USA
(310) 825-2879

ABSTRACT

In the Advanced Power Extraction (APEX) study, focus is placed on exploring innovative concepts for fusion power technology that can enhance the potential of fusion as an attractive and competitive energy source. The study will explore new and "revolutionary" concepts that can provide the capability to efficiently extract heat from systems with high neutron and surface heat loads while satisfying all other functional requirements (e.g. tritium self-sufficiency) and maximizing reliability, maintainability, safety, and environmental attractiveness. The minimum surface and neutrons wall load set for APEX study is ~1.5 MW/m2 and 7 MW/m2, respectively, with account taken for peaking factors. One of the concepts under investigation is flowing liquid layer in a once-though, top to bottom fashion, to protect the FW. This layer, while protecting the FW from exceeding the temperature and stress material limits under high power density conditions, will exhibit a rise in surface and bulk temperature whose magnitude depends on the mechanism of depositing both the surface and volumetric heat load. In the present study, several candidate materials for the liquid layer are considered, namely, lithium, Flibe, and Li17Pb83. The surface wall load is caused by the x-rays radiated from the hot plasma whose magnitude and spectrum strongly depends on the plasma operating conditions (e.g. electron temperature, impurities, etc.). On the other hand volumetric heating from incident neutrons is more or less deposited evenly through the layer with much lower steepness. In the present study, profiles of heat deposition rates from surface wall load of 1 MW/m2 are calculated for three liquid candidates up to a thickness of 5 cm. The spectrum of the classical Bremsstrahlung radiation is considered as the main constituent of this surface wall load and comparison is also made to the case where these x-rays are considered as mono-energetic energy source. Volumetric heating from neutrons are calculated for 7 MW/m2 wall load on a 5 cm-thick liquid layer followed by 50 cm-thick structure/coolant blanket region (20:80) that has a 15 cm-thick reflector zone (ferritic steel/water, 90:10) behind it. The combinations of liquid/blanket studied are Li/Li-(V-4Cr-4Ti) and Flibe/Flibe-(ferritic steel). Tritium production rate in these proposed layers and effect of Li-6 enrichment is also discussed. Exit and bulk temperature rise in the protective layer is discussed in a companion paper

I. INTRODUCTION

The initial driver of the APEX study is to develop a concept that has the capability for a high neutron wall load and associated surface heat flux. This stems from the fact that, as currently stands, the average core power density in present fusion reactors design is much lower than that in fission rectors (~0.4 MW/m3 in ITER for example vs. ~ 240 MW/m3 in LMFBR). The proposed High Power Density (HPD) concepts must satisfy the functional requirements of the Fusion Power Technology (FPT), namely, (1) provision of vacuum environment, (2) exhaust of plasma burn products, (3) power extraction from plasma particles and radiation, (4) power extraction from energy deposition of neutrons and secondary gamma rays, (5) tritium breeding at he rate required to satisfy tritium self-sufficiency, (6) tritium extraction and processing, and (7) radiation protection. The other most challenging issues in these HPD concepts are reducing components' failure rate (increasing mean time before failure, MTBF), increasing plant availability (reducing mean time to repair, MTTR), and satisfying tritium self-sufficiency requirement. The minimum neutron wall load for these concepts are: neutron wall load of 7 MW/m2 (average wall load of 5 MW/m^2, peaking factor of 1.4) and surface heat flux at the first wall. of at least 1.5 MW/m^2.

Thin and thick convective liquid layers that flow poloidally from the top to protect the first wall are among the several concepts under investigation. These concepts were recently investigated[1,4]. Liquid lithium, Flibe , and Li17Pb83 are candidates protective layers. In the present study, the Flibe Li2BeF4 was considered (rather than LiBF3) since it has 10 times lower viscosity but a high melting point of 460 °C. The surface wall load is caused by the x-rays radiated from the hot plasma. The spectrum of these rays depends on the plasma operating conditions (e.g. electron temperature, impurities, etc.) Most of the

emitted x-rays are in eV- keV energy range and photoelectric absorption is the main process for bearing with this surface wall load[5]. The steepness of power deposition depends on the x-rays attenuation properties inside the convective layer. Volumetric heating from incident neutrons, however, is deposited evenly through the layer with much lower steepness. Profiles of power deposition rate from 1 MW/m2 surface wall loads on layers up to 5 cm thick are given here with comparison to nuclear heating from 7 MW/m2 neutron wall load.

II. HEAT DEPOSITION PROFILES FROM X-RAYS

A. Mono-energetic X-Rays

Whether or not the surface load is absorbed at the surface or volumetrically distributed throughout the liquid layer, is mainly dependent on the x-rays attenuation characteristics of the type of layer under consideration. Figure 1 shows the attenuation length (in microns) versus photon energy (30 eV-30 keV) of x-rays incident perpendicularly on several materials. This length is defined as the penetration depth at which the photon intensity is 1/e of its initial incident value (i.e. equivalent to the mean free path $1/\Sigma$). Attenuation length for an incident angle θ is shorter by a factor of $\cos\theta$. Photon attenuation properties in materials can be found in Refs. 6-11.

The attenuation length for mono-energetic x-rays of 1 keV inside Li, Flibe, and Li17Pb83 are ~100, ~1, and ~0.12 microns, respectively. The corresponding length at 10 keV are ~1.3 x 10^5, ~1000, and ~10 microns. The attenuation coefficient of Li is ~ 2 orders of magnitude lower than in Flibe whereas the attenuation coefficient of Flibe is 1-2 orders of magnitude lower than in Li17Pb83. It is clear that Li exhibits larger attenuation depth (AD) followed by Flibe and Li17Pb83, in that order. Because of the very short attenuation length of x-rays in Li17Pb83, the present analysis focuses on profiles of heat deposition rate (HDR) in Li and Flibe and x-rays wall load in Li17Pb83 is considered to be deposited at the surface only. The larger attenuation length in Li resulted in an appreciably larger HDR than in the Flibe at larger depth. Figures 2 and 3 show the HDR profiles inside Li (ρ=0.534 g/cc) and Flibe (ρ =1.963 g/cc), respectively, for mono-energetic x-rays of various energies and for 1 MW/m2 surface wall load. For x-rays of 10 keV, HDR in Li and Flibe are 6.1 and 0.009 w/cc respectively at depth of 1 cm (6.5 and 1170 w/cc at surface). For the same x-rays energy, the HDR profile in Flibe is much steeper than in Li with much larger HDR at the surface. Figure 4 shows the depth in the layer at which a given fraction of the incident power is deposited. In a 5 cm-thick Flibe layer, 100% of the incident power is deposited within a depth of 10 micron, 0.01 cm, 0.06 cm, 0.2 cm, and 0.4 cm for 2, 4, 6, 8, and 10 keV x-rays. In Li, 100% of the power is deposited within 0.4 cm and 3.7 cm for 2 and 4 keV x-rays, respectively. For 6, 8 and 10 keV x-rays, ~84%, ~50%, and ~28% of the power is deposited in the 5 cm-thick layer (~16%, ~50%, and 72% fraction of power transmitted). This shows that Li is more transparent to x-rays than Flibe and volumetric heat deposition can be realized at measurable depth inside the Li layer. This transparency property is shown in Figs. 5 and 6 which depict the fraction of x-rays transmitted through a given layer thickness for photons of various energies. About 87% of the intensity (or power) of 10 keV mono-energetic x-rays can be realized behind a 2 cm-thick Li layer. This fraction is almost null in the case of Flibe. This fraction (87%) can be realized in Flibe after a thickness of 2 microns (2 x 10^{-4} cm) and for 25 keV x-rays, as can be seen from Fig. 5.

B. X-Rays from Classical Bremsstrahlung Radiation

Surface heating from plasma includes synchrotron and Bremsstrahlung radiation as well as line radiation from impurities[12]. For most part, the incident spectrum is mainly due to Bremsstrahlung with superimposed line spectra from impurities. For the sake of comparison with mono-energetic x-rays, the surface load is assumed to be constituted of Brem. radiation whose spectrum is function of the electron temperature Te. The spectrum of the classical Bremsstrahlung radiation is used as a representative spectrum and is given by:

$$Ex.\frac{dN}{dE_x} = \frac{a.n_e.n_i.g_{ff}.e^{-\frac{E_x}{T_e}}}{\sqrt{T_e}} \quad , T_e \text{ in eV, where} \qquad (1)$$

T_e = electron temperature

a = 9.6 x 10^{-20} $eV^{1/2}$ m^3 s^{-1}

g = Gaunt Factor ~ unity

Ex = x-rays energy, eV

dN/dEx = the number of quanta emitted per eV per second into 4π stredians by plasma of volume 1 m3.

The Brem. radiation power, P_{br}, is given by:

$$P_{br} = 5.35 \times 10^{-37} Z^2 \, ne \, n_z \, (Te)^{1/2}, \; W\,m^{-3}, \; Te \text{ in keV} \qquad (2)$$

Z = atomic number of ions

ne = electron density per m3

n_z = ni = ion density per m3.

Integrating Eq. (1) between Ex = 0 and Ex = ∞ gives Eq. (2) for Z=1. It can be shown that the fraction of x-rays in the energy range E_1 and E_2 is $\exp(-E_1/Te)-\exp(-E_2/Te)$.

Figure 7 shows the classical Brem. spectrum for various Te. The energy-integrated spectrum is shown in Fig. 8 as a function of the photon energy Ex. For Te= 10 keV, the fraction of spectrum below 100 and 300 eV is ~0.7% and ~2.5% respectively. The corresponding

fraction for Te=2 keV is ~3% and 12%, respectively. On the other hand, the fraction of spectrum above 10 keV is ~37% for Te= 10 keV and ~2% for Te= 2 keV. This has implication on the HPD profiles in the Li and Flibe layer.

C. Surface Heat Deposition Profiles in Li and Flibe

Figures 9 and 10 show the HDR from mono-energetic x-rays and Brem. spectrum at Ex/Te of 2 and 10 keV incident on Li and Flibe layer, respectively. At 10 keV, the mono-energetic x-rays has a more or less HDR of ~ 6 w/cc throughout the Li layer whereas the HDR for the Brem. spectrum peaks at the surface (HDR= ~9 x 10^4 w/cc) due to the low-energy component <100 eV. and is ~ 8 w/cc in the bulk of the layer. At 2 keV, the mono-energetic x-rays HDR profile is steep (~1.3 x 10^3 w/cc at surface and ~ 0.002 w/cc at 1 cm) whereas the Brem. spectrum has much larger HDR at the bulk of the layer (~6 w/cc at 1 cm) but still the low-energy component of the spectrum below 100 eV contributes appreciably to the HDR at the surface (~4 x 10^5 w/cc). These features are similar in the Flibe layer case but with much shorter depth as can be seen from Figure 10. The fact that the low-energy component of the Brem. spectrum contributes the most to the HDR near the surface is shown in Figure 11 where the HDR profiles from 30 energy bins, covering the range 30 eV- 30 keV,.are shown for Li. and for a depth of 1 cm. The corresponding profiles for the Flibe layer are shown in Figure 12.

The large HDR at the surface of the convective layer can be seen from Figure 13 which shows a comparison of the attainable HDR for mono-energetic x-rays and Brem. spectrum. The surface HDR drops faster with increasing the photon energy in the case of mono-energetic x-rays than in the case of Brem. spectrum (drops by ~2 orders of magnitudes in the former and by a factor of 4-5 in the latter as Ex/Te varies from 2 keV to 10 keV). For 10 keV, the surface HDR is ~ 9 x 10^4 w/cc in Li and 5 x 10^5 w/cc in Flibe. These large values are due to the absorption of low-energy tail of the Brem. spectrum below 80 eV in Li and ~ 200 eV in Flibe whose attenuation length is a fraction of a micron as can be seen from Fig. 1. This fraction of the spectrum is ~0.4% and ~2%, respectively. The HDR profiles near the surface and at the bulk of the protective layer are shown in Figs. 14 (depth of 5 cm) and 15 (depth of 0.03 cm). Clearly the surface temperature becomes larger as the fraction of the Brem. spectrum below 80 eV (Li) and 200 eV (Flibe) gets larger as in the case of Te=2 keV where this fraction is ~2% and ~10%, respectively (see Fig 8). *This suggests that part of the surface wall load can be treated as truly surface load whereas the rest of the incident load is considered to be deposited volumetrically throughout the protecting layer. The fraction that can be treated as a purely surface heat load (below 80 eV for Li and 200 eV for Flibe can be obtained from Fig. 8.*

From a practical design point, one would be interested in assessing the depth in the layer at which the HDR from surface wall load is comparable to the volumetric heating resulting from neutrons interaction with this layer. Figure 16 gives this depth in Li and Flibe for a 1 MW/m2 Brem. radiation of Te=2 and 10 keV. As shown, a 10w/cc is attainable at depth of ~0.9 cm (Li) and ~0.7 cm (Flibe) for Te=10 keV. Shorter depth is attainable for Te=2 keV (~0.8 cm and 0.1 cm, respectively). For a HDR of ~ 50-60 w/cc (which is comparable to neutrons/gamma heating at 7 MW/m2 neutron wall load, see next section), the depth for Te=10 keV is ~0.08-0.1 cm (Li) and 0.14-0.16 cm (Flibe). The corresponding depth for Te=2 keV is ~0.15-0.20 cm (Li) and ~0.04 (Flibe). Note that the HDR at and very near to the surface are higher in the Flibe layer than in the Li layer for Te=10 keV.

D. Surface Heat Deposition Profiles in Other Materials

Li17Pb83 is a candidate materials used in protecting the FW on one hand and in breeding tritium on the other. Because of the high effective Z number, the attenuation length is an order of magnitude less than in Flibe for 10 keV x-rays. SiC was proposed as the FW in ICF and the volumetric deposition of x-rays in that material has been explored[13]. Figure 17 shows a comparison of the attenuation length of x-rays in Vanadium, Iron, and SiC at several photon energies. at 10 keV, the attenuation length in SiC is ~120 microns as compared to ~12 microns in V and 0.8 microns in Fe. The HDR profiles from 1 MW/m2 classical Brem. radiation at Te=10 keV are shown in Fig. 18 where it is clear that this wall is deposited almost at the surface in the case of Li17Pb83 while sensible rates can be detected at deeper depths in the case of SiC. Further examination is underway to assess SiC as a FW material that can cope with high surface and neutron wall load without exceeding temperature and stress limits[14-15]

III. NUCLEAR HEAT DEPOSITION PROFILES

The 1-D calculational model used in the neutron/ gamma ray transport in the Li and Flibe system is shown in Fig. 19. On the outboard side, the 5 cm-thick convective layer is followed by a representative 50-cm-thick blanket and 15 cm-thick reflector zone. in the Li system, the blanket is made of Li:V4Cr4Ti (80:20) and made of Flibe:Ferritic Steel (80:20) in the Flibe system. The reflector considered in both systems is made of Ferritic Steel:water (90:10). It is included to neutronically account for neutron/gamma ray reflection, regardless of the compatibility concern. No breeding zone is considered on the Inboard side which includes a Be tile. The details of the TFC are considered in the model and the dimensions shown in Fig. 19 are those found at the mid plane in ITER configuration[16]. The analysis was

performed for 7 MW/m2 neutron wall load using ANISN transport code along with 175n-42g library based on FENDL/1.0 data[17] in P5S8 approximation.

The mean free path of neutrons (MFP=1/Σ) in Li, Flibe, and Li17Pb83 is shown in Figure 20 as a function of neutron energy. At 14 MeV, the MFP is ~ 16 cm in Li and 7 cm in Flibe. At all energies above ~ 3 eV, the MFP in lithium is larger than those in Flibe by as much as an order of magnitude . At thermal energies (below 1 eV) the MFP in lithium is a factor of ~6-8 lower than in Flibe. Thus, the lithium layer is much *more "transparent" to high-energy neutrons and much less "transparent" to low-energy neutrons* as compared to the Flibe. These features have direct impact on the nuclear heating rate throughout the system. neutron flux, the dpa, he-4, and h production rates in the walls of the V.V.

The maximum volumetric nuclear heat deposition rate (VNHDR) in the convective layer is larger in the Flibe than in the Li as can be seen from Fig. 21 which gives the VNHDR across the layer as a function of Li-6 enrichment. The Flibe-nat.Li6 and Flibe-25%Li6 profiles are similar to Li-50%Li6 and Li-90%li6 profiles. The maximum attainable VNHDR at the surface are:

	Flibe	Lithium
Natural Li-6	50 w/cc	38 w/cc
25% Li-6	55 w/cc	44 w/cc
50%Li-6	60 w/cc	49 w/cc
90%Li-6	64 w/cc	54 w/cc

It is larger in Flibe than in Lithium by as much as 30% (natural Li-6) to 18% (90% Li-6). The VNHDR increases in the layer as Li-6 enrichment increases due to the enhancement in Li-6(n,α) reaction which is exothermic (Q ~ 4 MeV). In the convective layer of Lithium, VNHDR is due mainly to neutrons heating. Non-negligible contribution from gamma heating exists in the case of Flibe. The profiles across the system are shown in Figs. 22 and 23 for the Lithium/(Li-V4Cr4Ti) and the Flibe/(Flibe-FS) case, respectively. The steepness of the profiles in Lithium/(Li-V4Cr4Ti) blanket is much less than in the Flibe/(Flibe-FS) blanket . This is due to the fact that more high-energy neutrons reach the blanket zone in the case of Li layer since the moderation power of Li is much less than Flibe for high energy neutrons (MFP is larger, see Fig. 20). Also, as the Li-6 increases, this high-energy component decreases at the back zones resulting in a less VNHDR at these back locations.

IV. TRITIUM PRODUCTION RATE (TPR)

The profiles for TPR in the convective layer are shown in Figs. 24 and 25 in the Li and Flibe system, respectively. The TPR from Li-6 is the main contributor to the integrated TPR (except in case of Li/(Li-V4Cr4Ti) blanket with natural Li-6 where contribution from Li-6 and Li-7 are comparable). In the convective Li layer (and the system), there is an optimal Li-6 enrichment (~ 25% Li-6) beyond which the integrated TPR begins to decrease. This is not the case for Flibe blanket where integrated TPR shows steady increase with Li-6 enrichment. There is a steepness in TPR profiles near the front surface of the convective layer due to Li-6(n,α) absorption of low-energy neutrons reflected to the layer by the Inboard blanket.

The total integrated TPR in the Li/(Li-V4Cr4Ti) system (Tritium breeding ration, TBR) is ~ 1.05 at 25% Li-6 enrichment (no T is bred in the I/B). The total integrated TPR in the Li layer is shown in Fig. 26 where contribution from Li-6 and Li-7 are also shown. Integrated TPR from Li-7 shows steady decrease with Li-6 enrichment whereas integrated TPR from Li-6 shows an optimal value at 25% Li-6 enrichment. The % contribution to the total TBR in the system from the Li layer is shown in Fig. 27. The 5 cm-thick Li layer contributes ~23% to the total TBR in the front 55 cm of the at all Li-6 enrichments. Note that the % contribution to total TBR from Li-7 increases with Li-6 enrichment and is ~ 35-37%. Most of the tritium from Li-7(n,n'α)t reactions is bred at the front locations where high-energy neutrons are found. The corresponding contribution in the Flibe/(Flibe-FS) system increase by enrichment (26%-32%).

The total TBR in the Flibe/(Flibe-FS) system is ~ 0.85 which is lower by ~ 25% than in the Li/(Li-V4Cr4Ti) system. Figure 28 shows the integrated TPR in the Flibe layer and the contribution from Li-6 and Li-7 tritium breeding reactions. As mentioned, there is a steady increase in the integrated TPR in the convective layer (and the system) with Li-6 enrichment. Figure 29 gives the % contribution to the total TBR from the Flibe layer which increases with Li-6 enrichment, being ~27% at natural Li-6 and ~ 31% at 90%Li-6 enrichment. Thus, for the same convective layer thickness, the contribution to the total TBR in the Flibe system is larger than in the Li system by ~ 5-7%. Note also that TBR from Li-7 in the Flibe layer is ~50% of the total TBR bred from Li-7 in the entire system. The values cited in the Flibe system does not account for tritium bred in the beryllium (one of the Flibe constituents).

V. SUMMARY

Innovative concepts are being explored and evaluated in APEX study to enhance the capability of removing high power density and surface wall load while satisfying all other blanket functional requirements (e.g. tritium self-sufficiency) and maximizing reliability, maintainability, safety, and environmental attractiveness. The minimum surface and neutrons wall load considered is ~1.5 MW/m2

and 7 MW/m2, respectively, with account taken for peaking factors. Liquid first wall is among the concepts considered in which a flowing layer is introduced from the top of the Tokamak to cope with the high surface and neutron wall load and to protect the blanket from excessive radiation damage. This convective layer will exhibit an increase in surface and bulk temperature as it flows poloidally to the bottom of the machine. Liquid lithium, Flibe, and Li17Pb83 are among the candidate materials considered. In the present work several issues were examined. They are: (a) attenuation characteristics and penetration range of the soft x-rays that carry most of the surface wall load, (b) profiles of heat deposition rate (HDR) from x-rays and from neutrons contributing to the rise in the convective layer temperature, and (c) tritium produced in the lithium-bearing layer relative to the total tritium bred in the system. In a companion paper[18] , the concept description and thermalhydraulics of liquid FW/Blanket are discussed based on the heat deposition characteristics assessed in the present work.

The attenuation length of 10 keV mono-energetic x-rays in Li, Flibe, and Li17Pb83 is ~1.3 x 10^5, ~1000, and ~10 microns, respectively, i.e., the attenuation coefficient of Li is ~ 2 orders of magnitude lower than Flibe whereas the attenuation coefficient of Flibe is 1-2 orders of magnitude lower than Li17Pb83. Thus, surface wall load could in principle be deposited volumetrically over a measurable depth in the convective layer of Li and to a lesser extent in Flibe while it is deposited at the surface in the case of Li17Pb83 due to its high attenuation coefficient. The incident x-rays consist mainly of Bremsstrahlung spectrum and line radiation from impurities and cover a wide range of energies in the eV-keV range. In the present study, classical Brem. radiation was considered at various electron temperature Te. For 10 keV Brem. radiation of 1 MW/m2, heat deposition rate (HDR) at the surface is ~ 9 x 10^4 w/cc in Li and 5 x 10^5 w/cc in Flibe. These large values are due to the absorption of low-energy tail of the Brem. spectrum below 80 eV in Li and ~ 200 eV in Flibe whose attenuation length is a fraction of a micron. This fraction of the spectrum is ~0.4% and ~2%, respectively. At the bulk of the layer, lower HDR are attainable at measurable depth. For example, at 1 cm depth, the HDR is ~10 w/cc (Li) and 8 w/cc (Flibe). For a HDR of ~ 50-60 w/cc (which is comparable to neutrons/gamma heating at 7 MW/m2 neutron wall load), the depth for Te=10 keV is ~0.1 cm (Li) and ~0.2 cm (Flibe). This suggests that part of the surface wall load can be treated as truly surface load whereas the rest of the surface load is considered to be deposited volumetrically.

Flibe is more powerful material in attenuating high-energy neutrons due to inelastic scattering in Fluorine and (n,2n) reactions in beryllium. For the same convective layer thickness and neutron wall load, nuclear heat deposited in the layer is larger in the Flibe case than Li by as much as It is larger in Flibe than in Lithium by as much as 30% (natural Li-6) to 18% (90% Li-6). The HDR increases in the layer as Li-6 enrichment increases due to the enhancement in Li-6(n,α) reaction. The steepness of the HDR profiles in Lithium/(Li-V4Cr4Ti) blanket is much less than in the Flibe/(Flibe-FS) blanket since more high-energy neutrons reach the blanket zone in the case of Li layer (Li is more "transparent" to high-energy neutrons and much less "transparent" to low-energy neutrons as compared to Flibe).

For a 5 cm-thick liquid FW, the total integrated tritium production rate (TPR) in the Li/(Li-V4Cr4Ti, 80:20) system (Tritium breeding ratio, TBR) is ~ 1.05 at 25% Li-6 enrichment (no T is bred in the I/B). Integrated TPR from Li-7 shows steady decrease with Li-6 enrichment whereas integrated TPR from Li-6 shows an optimal value at 25% Li-6 enrichment. The % contribution from the layer to the total TBR is ~23%. The TBR in the Flibe/(Flibe-FS: 80:20) system is ~ 0.85 which is lower by ~ 25% than in the Li/(Li-V4Cr4Ti) system. There is a steady increase in the integrated TPR in the convective layer (and the system) with Li-6 enrichment. The % contribution from the layer to the total TBR is ~27% at natural Li-6 and ~ 31% at 90%Li-6 enrichment. Thus, for the same convective layer thickness, the contribution to the total TBR in the Flibe system is larger than in the Li system by ~ 5-7%. Note that the representative blanket placed behind the 5 cm-thick liquid layer is not optimized for TBR nor tritium is bred in inboard blanket.

In the present work, the surface wall load is considered to be due to classical Bremsstrahlung spectrum. Actual spectrum should consider radiation from plasma impurities. Such radiation was recently assessed[19] in ITER using a circular plasma cylindrical with a radius of 4 m and is shown in Fig. 30[1]. An effort is underway to compare results based on this spectrum to the results cited in this manuscript.

---

[1] The volume and surface area for such a cylinder are 20% (volume) and 10% (surface) greater than for the actual ITER elliptical shape. The density profile was flat with n_e = 10^{20} m^{-3}. The temperature was parabolic (T_e = 20 keV (1-(r/a)^2)). The impurity mixture was 64 % H, 10 % He, 2 % Be, 1% C, and 0.2 % Ne. The radiation losses were mostly Bremsstrahlung, but there are losses from line radiation from the impurities and from radiative recombination. The line radiation losses are underestimated by perhaps as much as 50% or more because the calculation did not include transport effects".

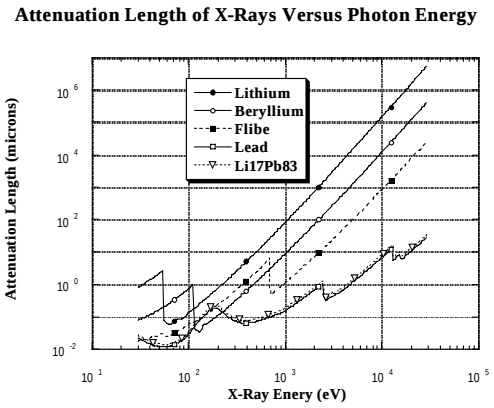

Figure 1: Attenuation Length of X-Rays In Lithium, Beryllium, Flibe, Lead, and Li17Pb83 VS. Photon Energy

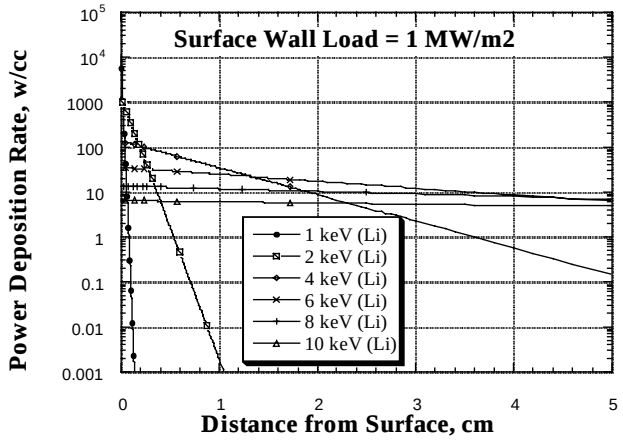

Figure 2: Power Deposition Profiles of Mono-Energetic X-Rays Incident on Lithium

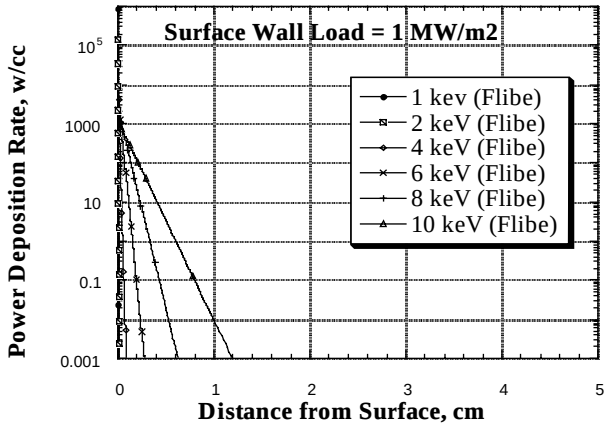

Figure 3: Power Deposition Profiles of Mono-Energetic X-Rays Incident on Flibe

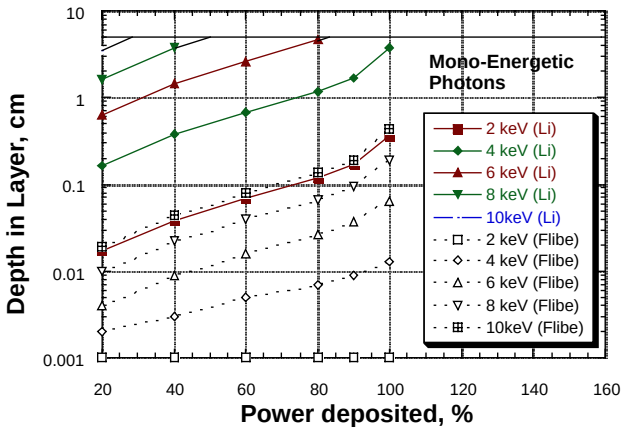

Figure 4: Depth in Convective Layer at which a given Fraction of Incident Power is Deposited from Mono-energetic X-Rays.

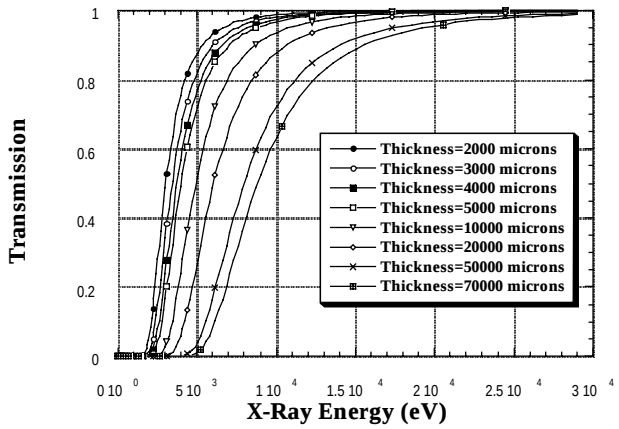

Figure 5: Fraction of Photons Transmitted Through Various Thickness in Lithium

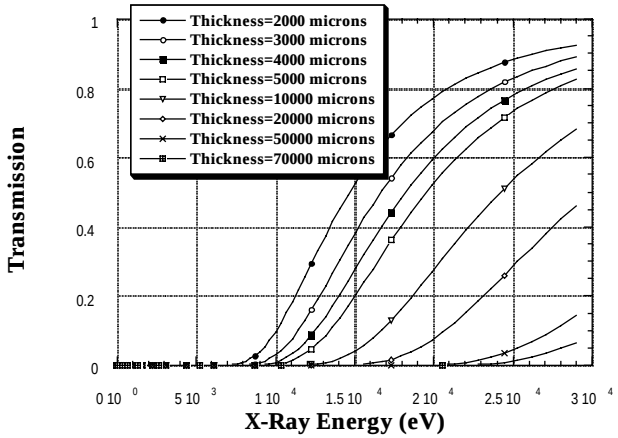

Figure 6: Fraction of Photons Transmitted Through Various Thickness in Flibe (Li2BeF4)

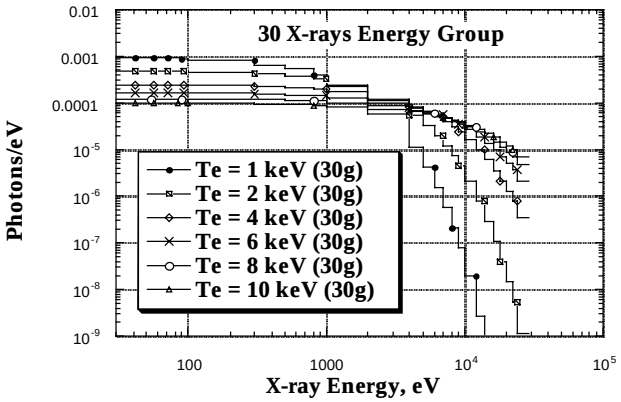

Figure 7: Classical Bremsstrahlung Spectrum at Various Electron Temperature (30 photon energy group)

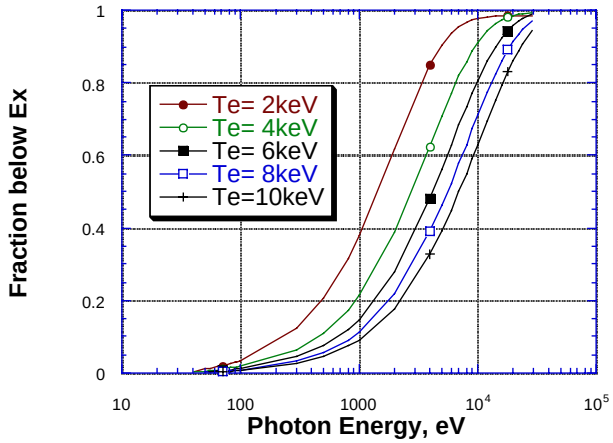

Figure 8: Integrated Classical Bremsstrahlung Spectrum at various Electron Temperature Te as a Function of Photon Energy Ex.

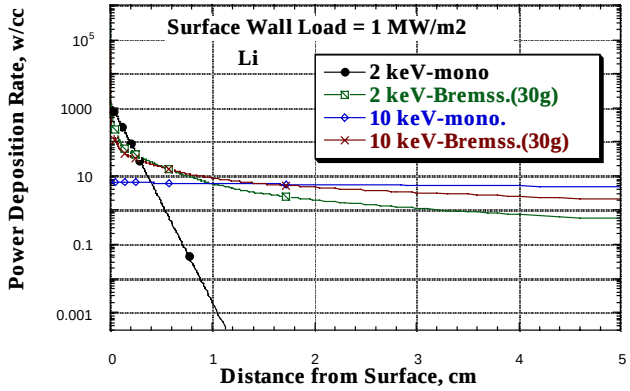

Figure 9: Comparison of Power Deposition Profile of Mono-energetic X-Rays of Te=2 and 10 keV and Classical Bremsstrahlung Spectrum Incident on Lithium (Depth = 5 cm)

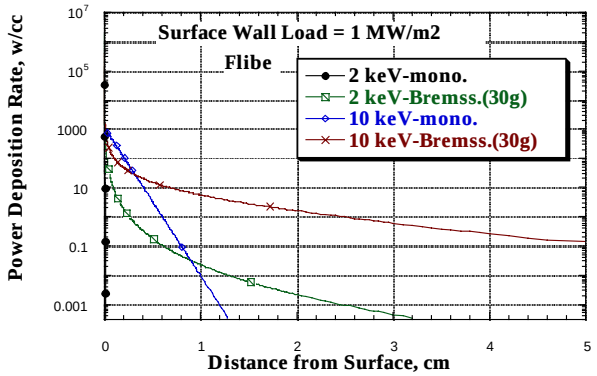

Figure 10: Comparison of Power Deposition Profile of Mono-energetic X-Rays of Te=2 and 10 keV and Classical Bremsstrahlung Spectrum Incident on Flibe (Depth = 5 cm)

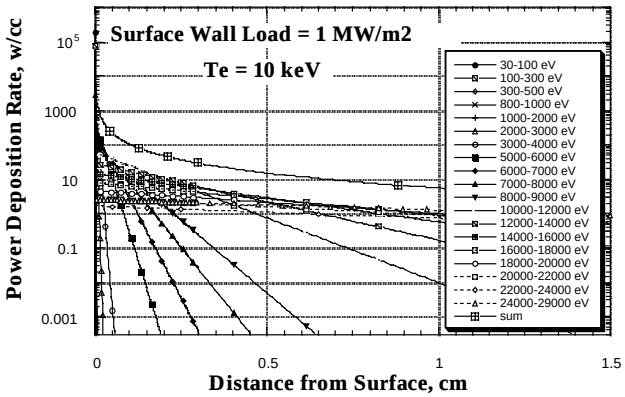

Figure 12: Power Deposition Profile and Contribution from Each x-ray Energy Range for Classical Bremsstrahlung Radiation Incident on Flibe (Depth = 1 cm)

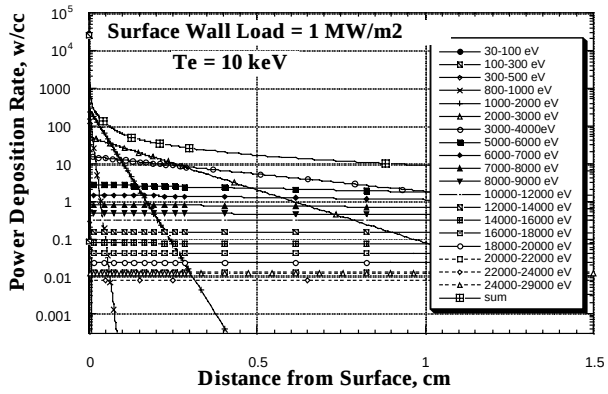

Figure 11: Power Deposition Profile and Contribution from Each x-ray Energy Range for Classical Bremsstrahlung Radiation Incident on Li (Depth = 1 cm)

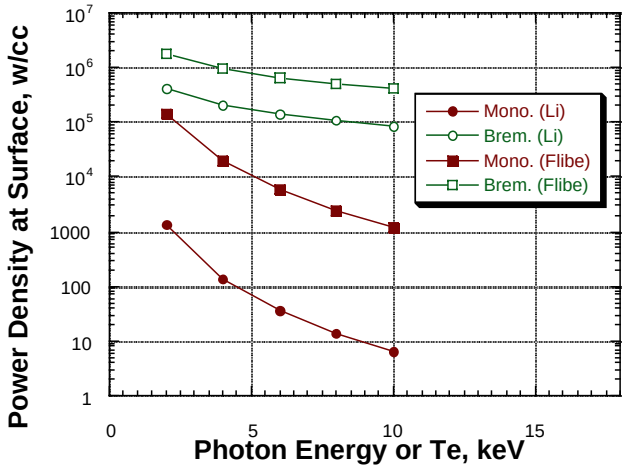

Figure 13: Surface Power Density from Mono-Energetic X-Rays and Bremsstrahlung Spectrum as a Function of Photon Energy/Electron Temperature Te

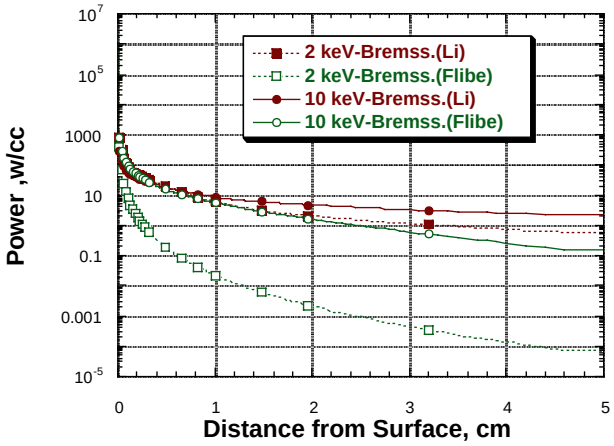

Figure 14: Power Deposition Rate from 1 MW/m2 Surface wall Load in Li and Flibe Convective Layer (Classical Bremsstrahlung Spectrum)-depth 5 cm

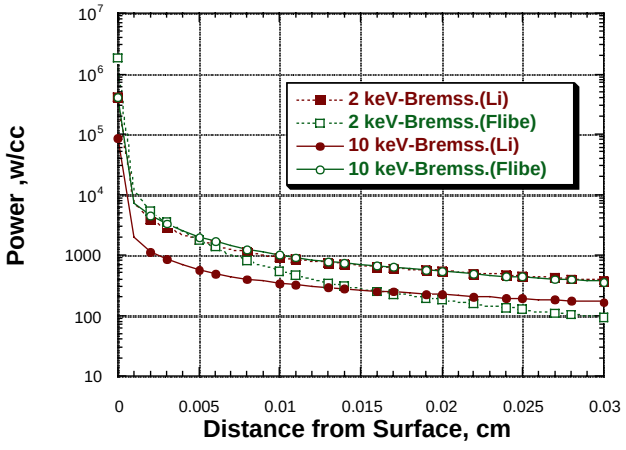

Figure 15: Power Deposition Rate from 1 MW/m2 Surface wall Load in Li and Flibe Convective Layer (Classical Bremsstrahlung Spectrum)-depth 0.03 cm

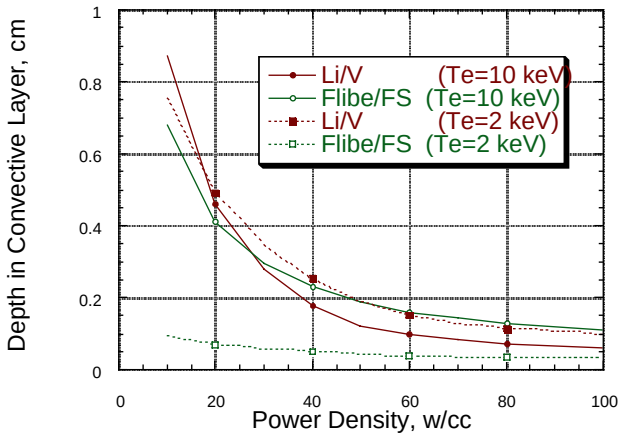

Figure 16: Depth in the Convective Layer as a Function of the Attainable Power Deposition Rate (Classical Bremsstrahlung Spectrum)

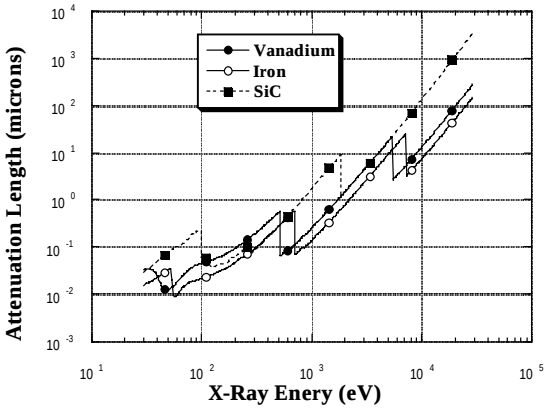

Figure 17: Attenuation Length of X-Rays In Vanadium, Iron, and SiC VS. Photon Energy

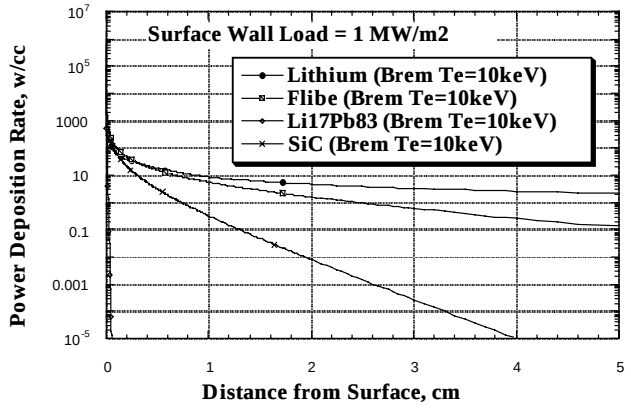

Figure 18: Comparison of Power Deposition Profiles from Classical Bremsstrahlung Radiation Incident on Several Materials (depth = 5 cm)

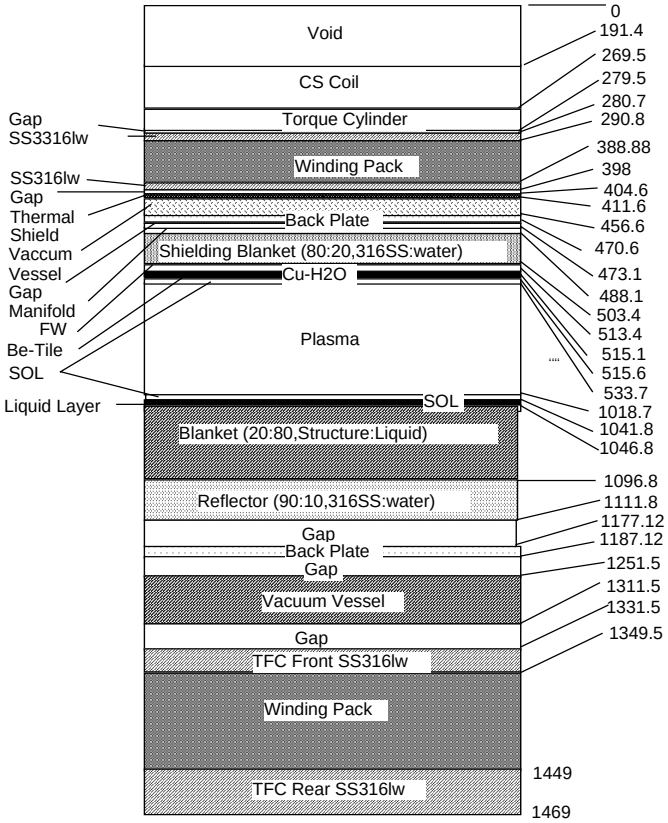

Figure 19: 1-D Calculational Model used in the Analysis

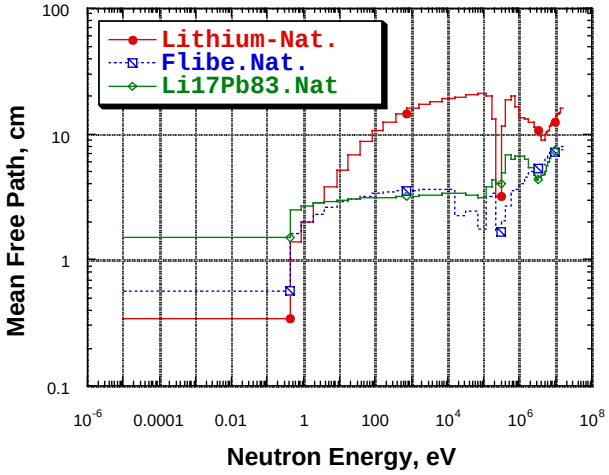

Figure 20: Neutron Mean Free path in Lithium, Flibe, and Li17Pb83

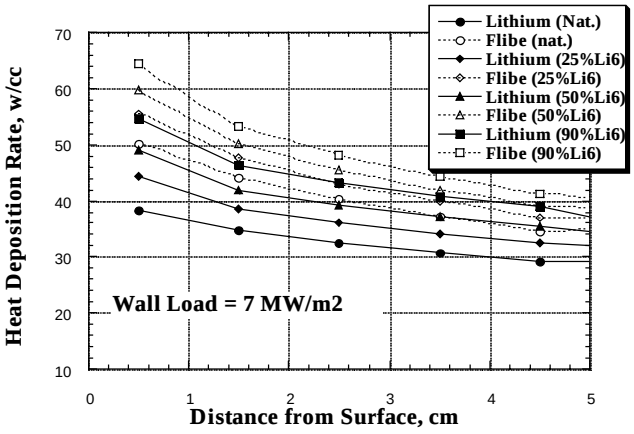

Figure 21: Comparison of the Volumetric Nuclear Heat Deposition Rate in the Convective Layer in Case of Lithium and Flibe for Various Li-6 Enrichment

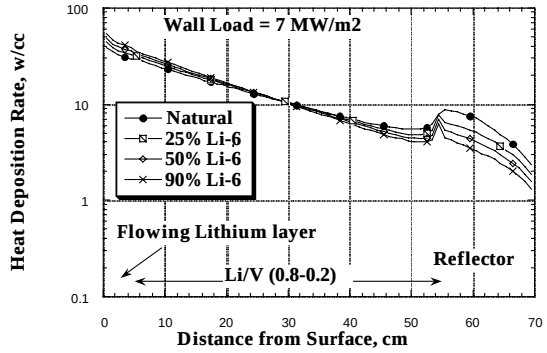

Figure 22: Volumetric Nuclear Heat Deposition Rate in the Li/(Li-V4Cr4Ti)/Reflector System

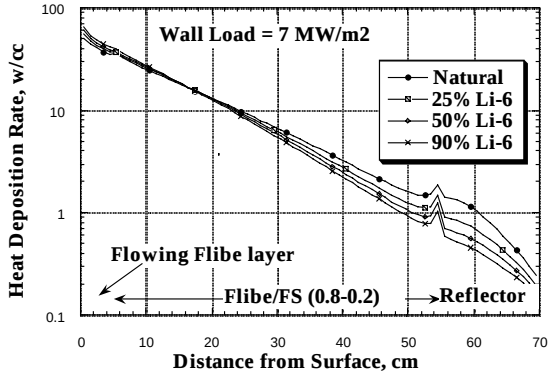

Figure 23: Volumetric Nuclear Heat Deposition Rate in the Flibe/(Flibe-FS)/Reflector System

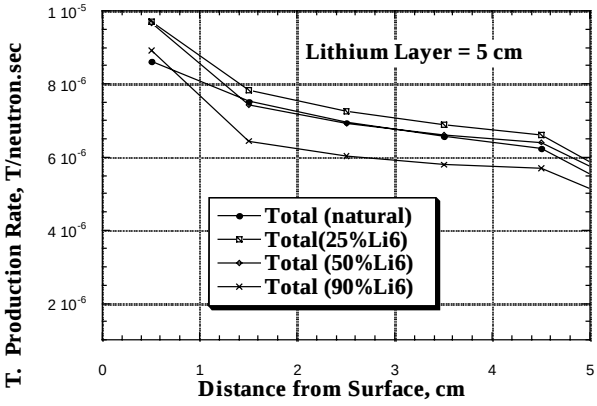

Figure 24: Total Tritium Production Rate in the Lithium Flowing Layer as a Function of Li-6 Enrichment

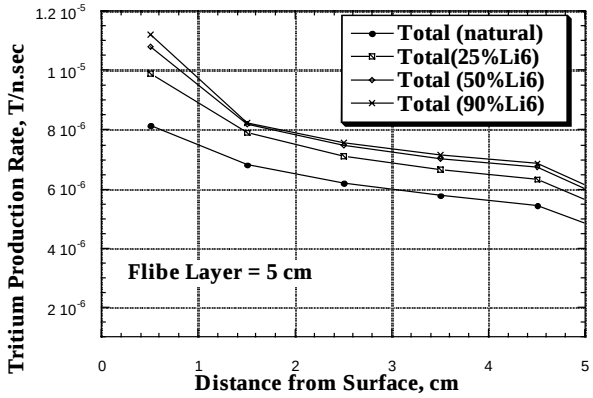

Figure 25: Total Tritium Production Rate in the Flibe Flowing Layer as a Function of Li-6 Enrichment

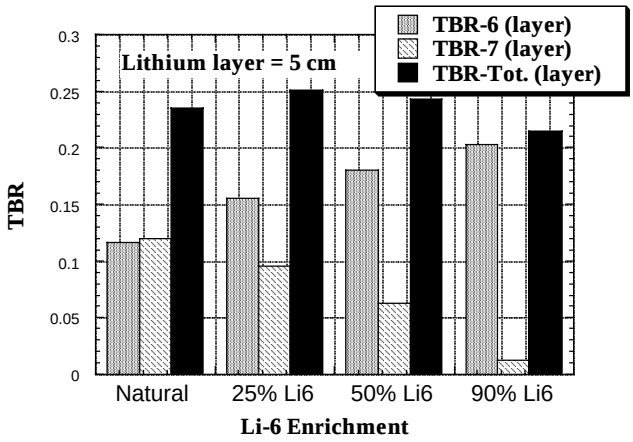

Figure 26: Tritium Breeding Ratio in the Convective Li Layer as a Function of Li-6 Enrichment.

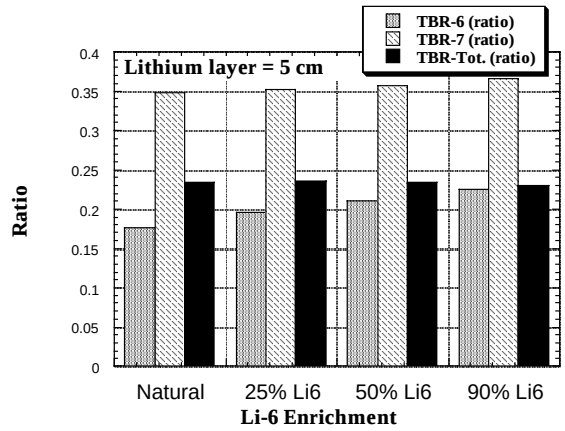

Figure 27: Ratio of Tritium Breeding in the Convective Layer to the System as a Function of Li-6 Enrichment (Lithium Flowing Layer)

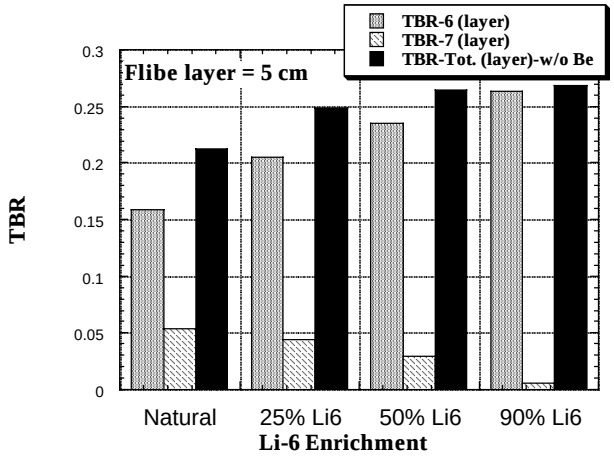

Figure 28: Tritium Breeding Ratio in the Convective Layer as a Function of Li-6 Enrichment (Flibe Flowing Layer)

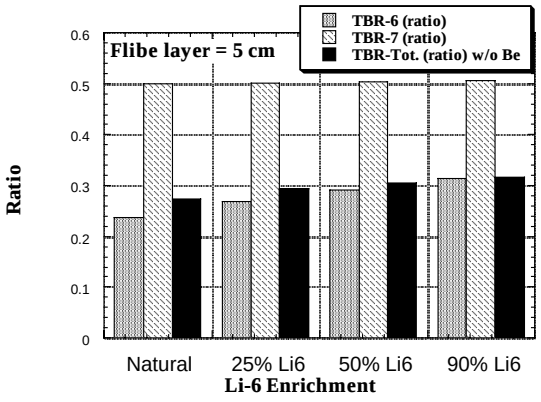

Figure 29: Ratio of Tritium Breeding in the Convective Layer to the System as a Function of Li-6 Enrichment (Flibe Flowing Layer)

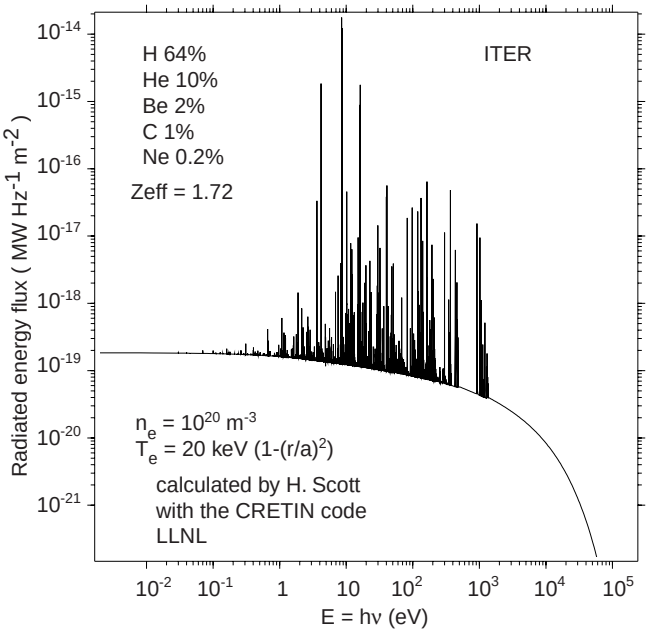

Figure 30. X ray and UV spectrum of the radiation losses from the ITER main plasma.

REFERENCES

1. R.W. Moir, "Liquid First Wall for Magnetic Fusion Energy Configuration", Nuclear Fusion, Vol. 37, No. 4, 1997.
2. N.C. Christofilos, J. Fusion Energy, 8 (1989) 97..
3. R.W. Moir, Fusion Eng. Des. 5, (1987) 269.
4. R.W. Moir, Nucl. Eng. Des. 29 (1995) 34
5. I. kaplan, "Nuclear Physics", Addison-Wesley Pub. Comp., INC., Reading Massachusetts, Palo Alto, London, (1964).
6. D.E. Cullen, et al., "Tables and Graphs of Photon Interaction Cross Sections from 10 eV to 100 GeV Derived from LLNL Evaluated Photon data Library (EPDL) Part A: Z = 1 to 50 and Part B: Z = 51 to 100, Vol. 6, Part A and Part B Rev. 4, Rep. UCRL-5000400, Lawrence Livermore National Laboratory, CA., 1989
7. J. A. Bearden and A. F. Burr Rev. Mod. Phys. 39, 125 (1967)
8. M. Cardona and L. Ley, Eds. Photoemission in Solids I. General Principles (Springer-Verlag, Berlin, 1978).
9. J. C. Fuggle and N. Martensson, J. Electron Spectrosc. Relat. Phenom. 21, 275 (1980).
10. S. Kraft, J. Stumpel, P. Becker, U. Kuetgens, Rev. Sci. Instrum. 67, 681 (1996).
11. J. R. De Laeter, K. G. Heumann, J. Phys. Chem. Ref. Data 20, 1313 (1991).
12. J. Wesson, "Tokamaks", Clarendon Press Oxford, (1987).
13. A. El-Azab and M.Z. Youssef," X-Ray Deposition in Inertial Fusion Graphite and Silicon-Carbide First Walls",

Proceedings of the 16th IEEE/NPSS Symposium on Fusion Engineering, 1995, pp. 33-36.
14. A. El-Azab and M.Z. Youssef, “X-Ray Absorption in Low-Z Materials and Impact on First Wall protection Schemes in Inertial Confinement Reactors, in these Proceedings.
15. A. El-Azab, private communication, University of California, Los Angeles, 1998.
16. “Technical Basis for ITER Detail Design Report, Cost Review, and Safety Analysis”. ITER Document, International Thermonuclear Experimental Reactor, (November, 1996).
17. A.B. Pashchenko, “Completion of FENDL-1 and Start of FENDL-2, INDC (NDS)-352, IAEA Nuclear Data Section, International Atomic Energy Agency, (March, 1996).
18. A. Ying, N. Morley, M. Youssef, K. Gulec, and M. Abdou, "Concept Description and Thermalhydraulics of Liquid Surface FW/Blankets for High Power Density Reactors", in these Proceedings.
19. D. Post, private communication, International Thermonuclear Experimental Reactor, ITER, San Diego Joint Working Site, U.S.A., ITER Memo, 9 January, 1998.